R9AP is a functional receptor for Epstein-Barr virus infection in both epithelial cells and B cells

Mu-Sheng Zeng (zengmsh@sysucc.org.cn)
Sun Yat-sen University Cancer Center https://orcid.org/0000-0003-3509-5591

li yan
Sun Yat-sen University Cancer Center

Hua Zhang
School of Medicine, Sun Yat-sen University

Xiao-Dong Dong
Sun Yat-sen University Cancer Center

Cong Sun
Sun Yat-sen University Cancer Center

Xiang-Wei Kong
Sun Yat-sen University Cancer Center

Dan-Ling Dai
Sun Yat-sen University Cancer Center

Qian-Ying Zhu
Sun Yat-sen University Cancer Center

Li Yuan
Sun Yat-sen University Cancer Center

Yu-Chun Li
School of Medicine, Sun Yat-sen University

Qian Zhong
Sun Yat-sen University Cancer Center https://orcid.org/0000-0003-1071-6996

Song Gao
State Key Laboratory of Oncology in South China, Collaborative Innovation Center for Cancer Medicine, Sun Yat-sen University Cancer Center, Guangzhou, 510060 https://orcid.org/0000-0001-7427-6681

Ya-Ping Tang
LSUHSC

Jin-Ying Yang
Guangzhou Women and Children's Medical Center, Guangzhou Medical University

Andrew McGuire
Fred Hutchinson Cancer Research Center https://orcid.org/0000-0003-1841-6859

Bo Zhao
Brigham and Women's Hospital, Harvard Medical School

Yi-Xin Zeng
Sun Yat-Sen University Cancer Center

Biological Sciences - Article

Keywords: Epstein-Barr virus, R9AP, epithelial cells, B cells

Posted Date: December 2nd, 2020

DOI: https://doi.org/10.21203/rs.3.rs-113641/v1

Abstract

Epstein-Barr virus (EBV), also known as the first human tumor virus, is linked to about 200,000 new cancer cases and millions of non-malignant diseases every year. EBV infects both human epithelial cells and B cells. Several virally encoded glycoproteins define tropism and mediate a complicated entry process. Here, we show that in both epithelial cells and B cells, R9AP silencing or genetic knockout significantly inhibits EBV infection, whereas R9AP overexpression promotes EBV infection, establishing R9AP as an essential entry receptor for EBV. Mechanistically, R9AP directly binds to EBV glycoproteins gH/gL to mediate membrane fusion. Importantly, the interaction of R9AP with gH/gL is inhibited by the highly potent, competitive gH/gL neutralizing antibody AMMO1 that blocks EBV infection of both epithelial cells and B cells. Furthermore, a R9AP peptide encompassing the gH/gL binding site inhibits EBV infection *in vitro* and reduces viral load in EBV infected humanized mice. Altogether, we propose R9AP as the first characterized receptor for EBV infection common to epithelial cells and B cells and a potential target for intervention.

Introduction

Epstein-Barr virus (EBV) is present in more than 90% of the global human population. In adolescents and young adults, primary EBV infection frequently caused infectious mononucleosis (IM)[1–3]. EBV is also involved in the development of autoimmune diseases, such as multiple sclerosis (MS). MS is the most common autoimmune disorder affecting the central nervous system[4–6]. Moreover, as the first virus discovered to cause human cancer, EBV is associated to ~200,000 new cancer cases annually, including B cell-derived malignancies, such as Burkitt lymphoma and Hodgkin lymphoma, as well as epithelial tumors, such as nasopharyngeal carcinoma (NPC) and EBV-positive gastric carcinoma[7–9]. Despite numerous breakthrough studies, there is still no licensed vaccine that can prevent primary EBV infection[10].

It has been suggested that EBV uses different combinations of viral glycoproteins to infect human epithelial cells and B cells[11]. The attachment of EBV to B cells depends on the interaction between EBV glycoprotein gp350 and B cell complement receptor CR2 (also known as CD21) or CD35[12,13]. Recently, CD21 also has been reported as the receptor interacting with EBV in T cells[14]. It has been proposed that EBV glycoprotein gp42, in complex with gH/gL, interacts with HLA class II to trigger the fusion activity of gB in B cells[15–17].

In contrast to B cells, epithelial cells lack not only CD21 and CD35 but also HLA class II[18,19], suggesting that EBV relies on different mechanisms and glycoproteins to infect epithelial cells[20–22]. The attachment of EBV to epithelial cells may involve EBV gH/gL or BMRF2 and their fusion may involve gH/gL and gB[11]. The interaction of EBV BMRF2 with integrins mediates virus attachment and entry to polarized epithelial cells[23]. EBV gH/gL also has been found to interact with integrins to trigger fusion[24,25]. We previously showed that gH/gL interacts with nonmuscle myosin heavy chain IIA (NMHC-IIA) to mediate EBV

attachment to B lymphoma Mo-MLV insertion region 1 homolog (Bmi1)-immortalized nasopharyngeal epithelial cells (NPECs) that grow as sphere-like cells (SLCs) instead of monolayer cells (MLCs)[26,27]. Currently, there is no evidence supporting a role of integrins or NMHC-IIA in EBV infection of B cells. Our previous work showed that neuropilin 1 (NRP1) could directly interact with EBV gB to promote EBV infection of NPECs but not B cells, which lack NRP1 expression[28]. Chen and we also identified ephrin receptor A2 (EphA2) bound to gH/gL and gB to serve as a receptor for epithelial cells but not B cells[29,30]. It is unknown if there are additional receptors that mediate EBV infection of epithelial cells.

As members of the "core fusion machinery" [31], gH/gL and gB are required for EBV to infect B cells and epithelial cells. Functional regions in EBV gH can be divided into four domains: domain (D)-I, D-II, D-III, and D-IV[32]. gL is important for gH folding and intertwines with gH D-I[33]. Several monoclonal antibodies have been identified to bind with different domains of gH to block EBV infection in either B cells or epithelial cells. However, AMMO1 is so far the only reported monoclonal antibody that binds gH/gL and blocks not only EBV infection of both epithelial cells and B cells *in vitro* but also EBV infection in animal infection models[34,35]. AMMO1 interacts with a discontinuous epitope among gH/gL D-I and D-II, but its precise mechanism of neutralization is unknown. It is possible that AMMO1 blocks the interaction of an unidentified common cellular factor with gH/gL. To identify the potential common cellular factor, we used cDNA microarray followed by siRNA screening and identified R9AP as a common receptor for EBV infection in both epithelial cells and B cells.

Results

R9AP promotes EBV infection

We reported that EBV infection efficiency was much higher in Bmi1-immortalized nasopharyngeal epithelial cells (NPECs) grown as sphere-like cells (SLCs) than as monolayer cells (MLCs)[27]. We speculated that some of the key factors that mediated EBV infection might be upregulated in SLCs than in MLCs. Thus, using microarray analysis we identified 132 genes that were upregulated in SLCs from two Bmi1-immortalized NPEC cell lines, namely NPEC1-Bmi1 and NPEC2-Bmi1 (Extended Data fig. 1, Supplementary Table 1). To identify the potential receptors or co-receptors associated with EBV infection, we performed a siRNA screening in SLCs targeting the 72 genes encoding membrane-associated proteins among these 132 genes with a pool of 4 siRNAs targeting each gene. The 72 siRNA pools were first transfected into NPEC2-Bmi1 MLCs, which were then grown as SLCs and infected with a recombinant EBV that expressed eGFP (EBfaV-GFP)[36]. EBV positive cells were identified by flow cytometry. By comparing the percentage of infected cells among the siRNA transfected cells with that of the control siRNA transfected cells, 10 genes were identified with a more than 50 percent reduction of EBV infection (Fig. 1a). These 10 siRNAs pools were then rescreened in NPEC1-Bmi1 cells for their effect on EBV infection. Targeting CNGA1, GPR1, SLC26A9 and R9AP were confirmed to reduce EBV infection more than 50 percent (Fig. 1b). RT-qPCR assay showed that each of these siRNAs pools efficiently depleted targeted genes expression (Extended Data fig. 2).

We next examined the expression of these genes in several cell lines that are susceptible to EBV infection. Western blotting showed that human B-cell lines, including EBV-positive Akata, EBV-negative Akata, and Raji, nasopharyngeal epithelial cell lines, including NPEC1-Bmi1, HNE1 and HK1, and the gastric epithelial cell line AGS consistently expressed CNGA1 and R9AP, but not GPR1 or SLC26A9 (Fig. 1c). To test whether overexpression of CNGA1 or R9AP could promote EBV infection, we transfected human embryonic kidney 293T (HEK-293T) cells with a construct expressing CNGA1 or R9AP (Fig. 1d). We found that overexpression of R9AP increased EBV infection more than 3 folds (Fig. 1e), we therefore selected R9AP for further investigation. A diagram summarizing the screening process is presented in Fig. 1f.

R9AP interacts with EBV gH/gL but not gB

EBV gH/gL and gB are considered to be necessary for EBV infection of both epithelial cells and B cells. To examine the potential interaction of R9AP with EBV envelope glycoproteins, co-immunoprecipitations were performed using HEK-293T cells transfected with a vector expressing FLAG-R9AP together with a vector expressing Myc-gH plus gL, Myc-gH alone, or Myc-gB or with an empty vector. Immunoprecipitation with anti-Myc antibody identified an association between gH/gL and R9AP but not gB. The interaction was strikingly reduced without the expression of gL (Fig. 2a), consistent with the notion that gL is essential for assisting the folding and transportation of gH[11]. Consistently, reverse immunoprecipitation with anti-FLAG antibody confirmed the interaction between gH/gL and R9AP (Fig. 2b). Purified recombinant His-gH/gL was pulled down by purified recombinant GST-R9AP$^{1\text{-}210}$, demonstrating a direct interaction between them (Fig. 2c). To further investigate whether R9AP could directly mediate EBV infection, the localization of EBV and R9AP was examined in HNE1 cells overexpressing R9AP. Confocal microscopy revealed that Alexa Fluor 594-labelled-EBV co-localized with eGFP-tagged R9AP (R9AP-eGFP) on the cell membrane and in the cytoplasm (Fig. 2d). Furthermore, Biolayer interferometry (BLI) also confirmed a direct interaction between R9AP and gH/gL by demonstrating high-affinity binding of GST-R9AP$^{1\text{-}210}$ to His-gH/gL (K_D=3.27E-09 M) (Fig. 2e). Taken together, these results demonstrated a strong, specific, and direct interaction between R9AP and gH/gL.

AMMO1 competes with R9AP for gH/gL binding

Because AMMO1 inhibits EBV infection of both epithelial cells and B cells, we hypothesized that its binding site on gH/gL might overlap with that of R9AP. To test this directly, a competition binding assay was performed using BLI. As a control, we included the anti-gH/gL antibody CL59, which binds to epitope located in gH D-IV and blocks EBV infection efficiently in epithelial cells but only partially in B cells[25,37]. An appropriate amount of His-gH/gL protein was first loaded on the Ni-NTA biosensor used for capturing His-tag-coupled protein. After a 30s of equilibration, the sensors were saturated with GST-R9AP or buffer intended for non-competitive control. The secondary binding of AMMO1 or CL59 to the biosensor was then monitored. To quantify the competition between each antibody and R9AP to the ligand gH/gL, raw signals of antibody binding were recorded with (Rc) or without (Ro) GST-R9AP association. Rc and Ro represent the responses of competitive binding and single ligand binding, respectively. The ratio of Rc/Ro reflects the intensity of competition. A ratio close to 1.0 indicates non-competitive binding and the

competition could be observed for ratio <0.7. Generally, a smaller value indicates a stronger competitive binding between ligands toward the targeted protein. Our findings showed that AMMO1 strongly competed with R9AP (Rc/Ro = 0.39) whereas CL59 did not (Rc/Ro = 1.02) (Fig. 2f).

To validate whether the interaction between gH/gL and R9AP could be blocked by gH/gL antibodies, co-immunoprecipitation was performed. gH/gL protein were pre-incubated with control IgG, AMMO1 or CL59 then mixed with R9AP. The results showed that AMMO1, but neither control IgG nor CL59, prevented the interaction between gH/gL and R9AP (Fig. 2g). Taken together, these results demonstrated that the AMMO1 overlaps with the R9AP binding site on gH/gL.

R9AP plays an essential role in EBV infection of both epithelial cells and B cells

Given above results, we further explored the role of R9AP in EBV infection in both epithelial cells and B cells. We first knocked down R9AP expression by siRNAs in nasopharyngeal epithelial HNE1 cells. Two independent siRNAs targeting R9AP significantly reduced R9AP expression (Fig. 3a). Consistently, the number of EBV-infected cells, which expressed eGFP, showed a remarkable reduction among R9AP knockdown cells by the visualization of fluorescence microscope (Fig. 3c). Meanwhile, the percentage of EBV-infected cells were determined by the flow cytometry analysis (Fig. 3a, b). The results showed that the efficiency of EBV infection was decreased at comparable levels in the R9AP knockdown cells. To exclude the potential siRNA off-target effects, we established *R9AP* genetic knockout HNE1 cells using CRISPR/Cas9. There was almost no detectable R9AP protein in the two sgRNAs (R9APsg1# and R9APsg2#) transfected HNE1 cells (Fig. 3d). Consequently, *R9AP* knockout almost abolished EBV infection in HNE1 cells (Fig. 3d). Importantly, the infection efficiency of *R9AP* knockout cells was mostly restored by ectopic expression of R9AP (Fig. 3e), indicating that the reduced EBV infection was not due to CRISPR off-target effect. R9AP knockdown in another nasopharyngeal epithelial HK1 cells also significantly inhibited EBV infection (Extended Data fig. 3).

In addition to NPC, almost ten percent of gastric adenocarcinomas are associated with EBV infection. To examine the role of R9AP in EBV infection of gastric epithelial cells, we knocked down R9AP in the gastric epithelial MKN74 cells (Fig. 3f) and found that MKN74 cells with reduced R9AP expression were less sensitive to EBV infection (Fig. 3f).

As B cells are among the primary host cells for EBV, we further examined the function of R9AP in EBV infection to B cells. To overcome the low transfection efficiency of siRNA in B cells, we established *R9AP* genetic knockout Raji cells with lentivirus expressing the same sgRNAs used in HNE1 cells and found that both sgRNAs reduced R9AP expression (Fig. 3g). Consistently, R9AP knockout inhibited EBV infection of Raji cells by 70-80% compared to the empty vector control (Fig. 3g). Taken together, these data indicated that R9AP is essential for EBV infection in both epithelial cells and B cells.

R9AP overexpression promotes EBV infection

We then examined whether overexpression of R9AP could increase EBV infection. We found that EBV infection was significantly increased in nasopharyngeal epithelial CNE1 cells and gastric epithelial AGS cells overexpressing R9AP (Fig. 4a). Overexpression of R9AP also increased EBV infection of EBV-negative Akata cells (Fig. 4b). Taken together, these results indicated that R9AP overexpression enhanced EBV infection of both epithelial and B cells.

R9AP mediates EBV fusion

Since AMMO1 inhibits the fusion of viral and cellular membranes, we further examined whether R9AP was required for fusion. Using cell-based EBV fusion assay, we found that EBV fusion was decreased in R9AP knockdown cells (Extended Data fig. 4a) but was increased in R9AP overexpressing cells (Extended Data fig. 4b). These results suggested that R9AP also affected the fusion of viral and cellular membranes.

The transmembrane, Habc Tri-helical Bundle domain and linker of R9AP are required for EBV infection

R9AP is a single-pass type □ transmembrane protein[38]. The wild-type (WT) R9AP includes 234 amino acids. According to the UniProt prediction[39], the R9AP transmembrane domain includes amino acids 211 to 231. Thus, we constructed truncated mutants that deleted the transmembrane domain and the three amino acids in C-terminal end ($R9AP^{1-210}$) or deleted only the amino acids in C-terminal end of R9AP ($R9AP^{1-231}$) (Fig. 4c). We then expressed the WT and the two truncated mutants in HEK-293T cells (Fig. 4c). Deletion of the 3 amino acids in the C-terminal end of R9AP did not affect EBV infection compared to WT (Fig. 4d). However, deletion of the transmembrane domain plus the C-terminal three amino acids remarkably decreased EBV infection compared to WT, indicating that anchoring of R9AP in the cellular membrane is crucial for EBV infection (Fig. 4d). The N-terminus of R9AP includes Habc putative trihelical bundle domain, linker and SNARE homology domain[39,40]. We further determined which domains of R9AP were responsible for EBV infection by creating a series of R9AP deletion mutants (Fig. 4e). Deletion of amino acids 1 to 50 or 101 to 152 in the Habc putative trihelical bundle domain and linker impaired the function of R9AP in allowing EBV infection. On the other hand, deletion of either amino acids 51 to 100 in the Habc putative trihelical bundle domain and linker or SNARE homology 153 to 200 did not affect EBV infection (Fig. 4f). The remarkable decrease in EBV infection of cells expressing R9AP lacking amino acids 1 to 50 compared to the WT indicated that the Habc Tri-helical Bundle domain was essential for EBV infection.

R9AP was assumed to anchor RGS9 to the disk membrane[38]. We used online software InterPro and TMHMM to predict the sub-cellular localization of R9AP[41,42]. Both websites predicted the N-terminal of R9AP as extracellular localization (Extended Data fig. 5a, b). To characterize the subcellular localization of R9AP, we expressed N-terminal Myc tagged amino acids 1 to 210 of R9AP ($Myc\text{-}R9AP^{1-210}$) or full-length R9AP ($Myc\text{-}R9AP^{FL}$) in HNE1 cells then stained them using anti-Myc antibodies, with or without permeabilization using Triton X-100 (TriX100). Without TriX100 treatment, only cells expressing $Myc\text{-}R9AP^{FL}$ were stained, not those expressing $Myc\text{-}R9AP^{1-210}$ (Extended Data fig. 5c). However, both cells

expressing Myc-R9AP^{FL} and those expressing Myc-R9AP$^{1-210}$ were stained after TriX100 treatment (Extended Data fig. 5c). Additionally, we observed endogenous R9AP by immunofluorescence staining with anti-R9AP antibody which targeting the N-terminus of R9AP in non-permeabilized HK1 cells (Extended Data fig. 5d). Together, these results indicated that N-terminal domain of R9AP could be exposed to cell surface.

Furthermore, we designed a biochemical experiment to confirm the extracellular localization of the R9AP's N-terminus by inserting a PreScission protease (PSP) -recognition site between the FLAG tag and N-terminal end of R9AP$^{1-210}$ (FLAG-psp-R9AP$^{1-210}$) or N-terminal end of R9AP^{FL} (FLAG-psp-R9AP^{FL}). When PSP was added outside fixed cells, the FLAG tag was removed only if the PSP recognition site was presented outside of cells, while not affected the binding site to the antibody against N-terminal of R9AP (Extended Data fig. 5e). Western blotting analysis showed that HNE1 expressing FLAG-psp-R9AP$^{1-210}$ presented similar amounts of truncated R9AP in the presence or absence of PSP, detected by either anti-FLAG or anti-R9AP antibodies, indicating the intracellular localization of the PSP recognition site in this truncated mutant. However, PSP treatment dramatically reduced FLAG-psp-R9AP^{FL} detection by anti-FLAG but not by anti-R9AP antibody (Extended Data fig. 5f), demonstrating that the N-terminal FLAG tag of FLAG-psp-R9AP^{FL} could be removed by PSP digestion and indicating that N-terminus of R9AP could be exposed outside the cells. Collectively, these results indicated that N-terminal domain of R9AP could locate at cell surface.

R9AP peptide impairs EBV infection *in vitro* and *in vivo*

Our results demonstrate that the N-terminal amino acids 1 to 50 of R9AP are essential for EBV infection. To determine whether peptides derived from this region could inhibit EBV infection, 5 peptides consisting of 1 to 12, 13 to 24, 19 to 30, 30 to 41, and 35 to 46 amino acids of R9AP (R9AP$^{1-12}$, R9AP$^{13-24}$, R9AP$^{19-30}$, R9AP$^{30-41}$ and R9AP$^{35-46}$) and a scrambled control peptide were synthesized. EBV was first incubated with each peptide at 4°C for 2h then used to infect HNE1 cells at 37°C for 3h. After 24 h, EBV positive cells were analyzed by flow cytometry. We observed that R9AP$^{19-30}$ peptide inhibited EBV infection in a dose-dependent manner (Fig. 5a). Consistently, R9AP$^{19-30}$ peptide also markedly reduced EBV infection in Raji cells (Fig. 5b). BLI was also performed to detect the specific affinity of R9AP$^{19-30}$ peptide to gH/gL. Results showed that the binding of R9AP$^{19-30}$ peptide to gH/gL was significantly stronger than the scrambled control peptide, which indicating a strong and specific binding to gH/gL (Fig. 5c). In summary, these results indicated that R9AP$^{19-30}$ peptide inhibited EBV infection in both epithelial cells and B cells.

Next, we evaluated the *in vivo* effect of R9AP$^{19-30}$ peptide against EBV infection in humanized mice. It was reported that SCID mice developed post-transplant lymphoproliferative disorders (PTLD) after reconstitution by intraperitoneal human peripheral blood mononuclear cell (PBMC) injection followed by EBV infection[43,44]. Previous studies also found that cord blood cells infected with EBV *in vitro* induced lymphomas when injected into NSG mice[45,46]. We reconstituted B-NDG mice by intraperitoneal injection of cord blood cells. Subsequently, EBV and peptide were simultaneously injected into the mice through

their tail vain on day 0. Then, the mice were intraperitoneally administered with R9AP$^{19-30}$ peptide or control peptide at 20mg/kg on days 3, 7 and 14 (Fig. 5d). The engrafted T cells were able to slow the growth of EBV-induced lymphomas in a Cord Blood Humanized-Mouse Model[46]. To inhibit engrafted T cell function, T cell depleting monoclonal antibody (OKT3) was injected into the mice on day 7 after EBV injection. The peripheral blood of infected mice was collected at indicated time. EBV DNA in the peripheral blood was first detected 4 weeks after inoculation and was observed to increase rapidly. EBV copy number was much lower in mice treated with R9AP$^{19-30}$ peptide compared to those treated with the control peptide on the 6th week after injection (Fig. 5e). The death of mice first appeared on day 43 after EBV injection. Mice treated with R9AP$^{19-30}$ peptide survived longer than those treated with control peptide (Fig. 5f). However, there was no apparent difference in body weight between mice treated with the control and those treated with the R9AP$^{19-30}$ peptide (Extended Data fig. 6a). Human CD20 and the latent EBV non-coding nuclear RNAs (EBERs) were detected in the spleens of all mice (Extended Data fig. 6b), which indicated the successful construction of EBV infecting B-NDG mice model. However, the proportion of EBERs-positive cells in R9AP$^{19-30}$ peptide treated mice was much lower than the control peptide treated mice (Extended Data fig. 6c). These data implied that R9AP$^{19-30}$ peptide protected mice against EBV infection *in vivo* and that targeting R9AP could be a potential strategy against EBV infection.

The expression of R9AP in tissues susceptible to EBV infection

Primary EBV infection is commonly thought to occur *in vivo* in the oropharynx, after which the virus spreads throughout the lymphoid tissues to infect B cells[47]. To determine the expression of R9AP in these tissues, we performed immunohistochemical (IHC) staining for R9AP in human tongue, floor of the mouth and lymphoid tissues. Human retina and liver tissues were used as positive and negative control, respectively[40,48]. As expected, R9AP mainly was found in the outer segment layer of retina, while not detected in the liver tissues (Extended Data fig. 7). We observed that R9AP-positive cells mainly distributed in the basal layer of stratified squamous epitheliums in the tongue and floor of the mouth as well as in follicular areas of lymphoid tissues in all five investigated specimens of each tissue (Fig. 6a). Four of 5 pseudostratified ciliated columnar epithelium of the nasopharynx stained weakly. Dysplastic nasopharyngeal epithelium tissues were found to become susceptible to EBV infection compared to the normal nasopharyngeal epithelium tissues[47,49]. Consistently, 3 of 4 dysplastic nasopharyngeal epithelium tissues stained strongly for R9AP (Extended Data fig. 8). However, R9AP was undetectable in all 5 of normal glandular epithelium of the stomach tissues (Extended Data fig. 8). It was noteworthy that R9AP and EBERs could be detected, in similar distribution patterns in consecutive sections, in all analyzed EBV-associated human tumor samples, including 5 NPC specimens, 3 EBV-positive gastric carcinoma specimens, and 4 EBV-positive B cell lymphoma specimens (Fig. 6b).

Discussion

As a member of the herpesvirus family, EBV requires the coordination of a set of envelope glycoproteins and corresponding cellular receptors or co-receptors to efficiently infect host cells. To identify membrane-

associated proteins that are important for EBV infection, we used unbiased transcriptomic microarray analysis combined with a siRNA library screening based on a highly efficient EBV infection model that we previously reported[27]. As far as we know, we identified R9AP as the first characterized receptor to mediate EBV infection of both epithelial cells and B cells, which are the major cell types infected and potentially transformed to malignancy by EBV.

R9AP mediated EBV infection of both epithelial cells and B cells. Several molecules, such as CD21, CD35 and MHC-II, have been identified as B cells' receptors or co-receptors for EBV infection[12,13,16,17], we and others identified EphA2, NRP1, NMHC-IIA, and integrins as receptors or co-receptors for EBV infection in epithelial cells[24,25,27–30]. However, none of the above identified receptors were shared by epithelial cells and B cells. Although we first characterized the importance of R9AP in EBV infection of nasopharyngeal epithelial cells, we have validated that R9AP plays an essential role in EBV infection of gastric epithelial cells and B cells. Recently, CD21 was reported to mediate EBV infection in T lymphocytes[14]. R9AP is also expressed in human T cells and natural killer (NK) cells according to human protein atlas (HPA) datasets[48]. However, it requires further investigation if R9AP plays a role in EBV infection of NK/T cells.

Enveloped virus entering host cells can be divided into two steps: virus first binding to the cell surface, then fusing with cell membrane and penetrating to release the capsid and nucleus into cytoplasm[11]. It was generally believed the B cell infection was initiated by EBV gp350 attachment to CD21, possibly allowing gp42 interaction with HLA class II. This close membrane protein interaction would trigger core fusion complex gH/gL and gB to fulfill final viral-host membrane fusion[31]. We previously identified EphA2 and NRP1 as gH/gL or gB receptors for EBV fusion in epithelial cells. It remained unknown whether there are gH/gL or gB receptors for EBV fusion in B cells. Our results demonstrated that R9AP mediated EBV fusion through its interaction with gH/gL, which helps to fully understand the fusion mechanism. As mentioned above, several host factors have been found during different steps of EBV infection in either B cells or epithelial cells. Further studies will be needed to elucidate the relationship between R9AP and these host factors during EBV infection.

The competition between AMMO1 and R9AP to gH/gL binding facilitate the delineation of the mechanism of AMMO1-mediated neutralization. Previous study found that EBV lacking gH failed to infect both epithelial cells and B cells[50], which indicates the indispensable role of gH in EBV infection. As expected, the human neutralizing antibody AMMO1, which binds to gH/gL D-I to D-II, can block EBV infection of both B cells and epithelial cells[34,35], but the precise mechanism of neutralization was unknown. These results suggest a potential gH/gL receptor that might be used during EBV infection of epithelial cells and B cells. However, a gH/gL receptor in B cells or shared by epithelial cells and B cells remains unidentified for a long time. Our results found the interaction between R9AP and gH/gL was specific and could be inhibited by AMMO1, which suggests that this is the mechanism of AMMO1-mediated neutralization. These findings also support the notion that vaccines designed to elicit antibodies targeting gH/gL and thus blocking the interaction between gH/gL and R9AP could raise the

possibility to prevent EBV infection in both epithelial and B cells, thus reducing the incidence of EBV associated diseases.

R9AP is a potential target against EBV infection. Acute EBV infection causes infectious mononucleosis, EBV also reactivates in a subset of individuals with cancers, autoimmune diseases and organ transplantation et al.[1,2,51–53]. Although recent development of preclinical small molecule targeting EBNA1 seemed to show promise as a potent anti-EBV drug, no specific anti-EBV drug is available in clinic[54,55]. Importantly, both *in vitro* and *in vivo* experiments demonstrate a peptide to mimic R9AP 19 to 30 amino acids could inhibit EBV infection. Given that loss of function mutations in this gene are not lethal, and are only associated with bradyopsia[56,57], it may be safe to transiently inhibit R9AP's function in order to block EBV infection in these diseases.

Taken together, our findings suggest that R9AP is the first characterized receptor to mediate EBV infection in both epithelial and B cells, which have a great implication for the development of vaccines and therapies against EBV infection.

Materials And Methods

Cell lines. Bmi1 immortalized nasopharyngeal epithelial cells (NPECs-Bmi1) were cultured in keratinocyte serum-free medium (17005-075; Invitrogen, California). The NPECs-Bmi1 monolayer cells (MLCs) and sphere-like cells (SLCs) were formed according to a published protocol[27]. Briefly, 5×10^4 or 5×10^5 NPECs-Bmi1 cells were seeded into 48-well plates and cultured for 36 h. Cells seeded at 5×10^4 per well turned to grow as MLCs, while cells seeded at 5×10^5 per well grew as SLCs. Human embryonic kidney 293T (HEK-293T) cells were grown in DMEM (C11995500BT; GIBCO, California) supplemented with 10% (vol/vol) FBS (10099-141C; GIBCO, Australia). HNE1, HK1, CNE1, AGS, Raji, MKN74 and Akata cells were maintained in RPMI medium 1640 (C11875500BT; GIBCO, California) supplemented with 5% (vol/vol) FBS. All cells were cultured at 37 °C in a humidified atmosphere comprising 5% CO_2 incubators. HEK-293T cells were purchased from ATCC; NPECs-Bmi1 were established by our laboratory as described before (*26*); CNE1 cells were a kind gift from Professor Quen-Tin Liu (Sun Yat-sen University, Guangzhou, China); HNE1 and HK1 cells were a kind gift from Professor Sai-Wah Tsao (University of Hong Kong, Hong Kong SAR); AGS cells were a kind gift from Professor Qian Tao (Chinese university of Hong Kong, Hong Kong SAR); MKN74 cells were a kind gift from Professor Xu Rui-Hua (Sun Yat-sen University, Guangzhou, China); EBV-positive Akata cells were a kind gift from Professor Maria G. Masucci (Karolinska Institute, Sweden).

Reagents: Peptides based on amino acids 1 to 50 of R9AP, including $R9AP^{1-12}$ (MAREECKALLDG), $R9AP^{13-24}$ (LNKTTACYHHLV), $R9AP^{19-30}$ (CYHHLVLTVGGS), $R9AP^{30-41}$ (SADSQNLRQELQ), and $R9AP^{35-46}$ (NLRQELQKTRQK), as well as a scrambled control peptide (LVHYTHCGSLGV) were synthesized by CHINESE PEPTIDE (China). The rabbit anti-R9AP antibody used for Western blotting (WB),

immunofluorescence staining and immunohistochemistry staining was purchased from Sigma-Aldrich (HPA049791, Germany). AMMO1 and CL59 antibodies were a kind gift from Professor Andrew T. McGuire (University of Washington) and Professor Richard Longnecker (Northwestern University), respectively. PreScission protease (PSP) was a kind gift from Professor Song Gao (Sun Yat-sen University Cancer Center). All other reagents were obtained from Sigma-Aldrich, unless indicated otherwise.

Microarray analysis. NPECs-Bmi1 MLCs and SLCs were formed, then, total RNA was extracted using TRIzol reagent (T9424; Sigma-Aldrich, Germany), according to the manufacturer's instructions. The integrity of the RNA was checked on a Bioanalyzer 2100 (Agilent Technologies, USA). The microarray experiments were performed by Shanghai Biochip Corporation (Shanghai; China) using the Agilent Whole Human Genome Oligo Microarray 4×44K (Agilent Technologies, California). The cRNA synthesis, cRNA labelling, sample fragmentation, and microarray hybridization were performed based on the manufacturer's standard protocols. The arrays were scanned using the Agilent Scanner G2505B (Agilent Technologies, California). Feature Extraction software (version 9.5.3.1, Agilent Technologies) was used to obtain raw data, which were normalized using the quantile algorithm in Genespring (version 9, Agilent Technologies). Differentially expressed genes were then selected according to the threshold set as fold change > = 2.0 and a P value < 0.05 according to the *t*-test. The identified differentially expressed genes were then subjected to GO (Gene Ontology) and KEGG (Kyoto Encyclopedia of Genes and Genomes) pathway enrichment analysis. The microarray data were deposited with the NCBI GEO depository under the accession number of GSE159958. The zipped data includes raw data from the microarray for each sample, the normalized expression matrix of genes from all samples, and per-sample metadata. Differentially expressed genes were selected according to the threshold set as fold change >2.0 and a P value <0.05 by *t*-test. The bioinformatics analysis of differentially expression genes were conducted by GO (Gene Ontology) and KEGG (Kyoto Encyclopedia of Genes and Genomes) analysis. The heatmap was generated using GraphPad Prism software.

Gene silencing. ON-TARGET plus SMART pool siRNAs against 72 upregulated membrane-associated genes and ON-TARGET plus siCONTROL Non-Targeting pool siRNA which was used as control were all purchased from GE Dharmacon (California). The two single siRNA duplexes against R9AP were as follows:

R9APsi1#:5'-GCGAGAUGAUCGACAACAU-3'; R9APsi2#:5'-GCAAAAGACGCGCCAGAAG-3'; All the siRNAs were delivered using RNAi MAX (13778150; Invitrogen, California) according to the kit instructions.

Generation of isogenic R9AP knockout cell lines. The generation of R9AP HNE1 and Raji knockout cell lines was based on CRISPR-Cas9 gene editing technology. The guide RNA (gRNA) sequences were 5'-

CGAGTCCGCCGAGCCACCGA-3’ (R9APsg1#) and 5’- GCTGACCGTCGGTGGCTCGG-3’ (R9APsg2#). Oligonucleotides corresponding to the gRNA were synthesized and cloned into Cas9-expressing plasmid PX459 (48139, Addgene, Massachusetts) or lentiCRISPRv2 (52961, Addgene, Massachusetts). HNE1 cells were transiently transfected with R9AP gRNA cloned into pX459 using Lipofectamine 3000 transfection reagent (L3000015; Invitrogen, California). After 24h, transfected cells were selected using puromycin (60210ES80; Yeasen, China) at 1μg ml^{-1} for 3 days. Raji cells were infected with lentivirus encoding R9AP gRNA, and after 24h, the infected cells were selected using puromycin (1 μg ml^{-1}) for 3 days.

Expression of cDNA. The indicated plasmids were delivered using Lipofectamine3000 following the instructions. The establishment of R9AP stable expression EBV-negative Akata cells was based on the pBABE-Puro Retroviral system (RTV-001-puro, Cell BioLabs, California).

***In vitro* EBV infection**. The utilized EBV containing eGFP (EBfaV-GFP), was prepared in EBV-positive Akata cells[36]. EBV production, labeling, and determination of MOI and infectious particles were performed as reported previously[27,28]. SLCs of NPECs-Bmi1 and HEK-293T were infected with EBV at an MOI of ≈300; HNE1, HK1, CNE1, AGS, MKN74, Raji and EBV-negative Akata cells cells were infected with EBV at an MOI of ≈1000. The indicated cell lines were incubated with EBV for 3h at 37°C, and unbound virus was discarded by washing with PBS three times. Then, cells were cultured in fresh medium for 24h, followed by quantification of eGFP positive cells using flow cytometry (cytoFLEX; Beckman).

Fusion assay. The virus-free cell fusion assay was performed according to previous published protocol (*30*). Effector HEK-293T cells were transfected with T7 luciferase reporter plasmids with a T7 promoter, gB, gH and gL. Renilla luciferase was used as internal control. To examine the effects on fusion after expressing R9AP, target HEK-293T cells were transfected with the T7 DNA polymerase expression plasmid together with the R9AP expression plasmid or empty vector. To test the effects on fusion after R9AP knockdown, target HEK-293T cells were transfected with R9AP siRNA or the control siRNA, followed by transfected with the T7 DNA polymerase expression plasmid 36h later. After 24h, 2.5×10^5 effector HEK-293T cells were mixed with 2.5×10^5 target HEK-293T cells in 24-well plates and cultured for another 24h. The luciferase activity was measured via a dual-luciferase reporter assay system (E2920, Promega, Wisconsin) using the GloMax-96 Microplate Luminometer. The ratio of firefly luciferase activity to Renilla luciferase activity was used as the relative fusion activity.

Peptide blocking assay. EBV was pre-incubated at 4°C for 2h with either $R9AP^{1-12}$, $R9AP^{13-24}$, $R9AP^{19-30}$, $R9AP^{30-41}$ or $R9AP^{35-46}$ peptide which was diluted to the concentration of 100 and 200μg mL^{-1} in FBS-free

RPMI 1640, and then added to the cells. The scramble control peptide at 200μg mL^{-1} was used as control. Cells were treated with EBV at 37°C for 3h and subsequently washed three times by PBS. The percentage of EBV-infected cells was determined by flow cytometry at 24h post infection.

Protein expression and purification. GST-R9AP$^{1-210}$ was expressed in *E.coli* BL21 (AI) cells (CB105-02; Tiangen, China). The cells were cultured on TB plates containing 0.1mg/L of ampicillin (A010-10g; MDbio, China) at 37°C overnight. A single colony was picked and transfected into liquid TB medium supplemented with ampicillin for expansion until an appropriate OD value (0.6-0.8) was reached. The culture was then cooled down to 18 °C and isopropyl-thio-β-D-galactopyranoside (IPTG; 1122GR025; BioFroxx, China) was added to a final concentration of 0.2mM to induce protein expression, which was continued for 8 hours at 18°C. The cells were then collected by centrifugation and resuspended in PBS, pH 7.4 containing Roche's complete Protease Inhibitor (EDTA-free) (11697498001; Roche, Switzerland). Then, the cells were lysed by pressured crushing at 4°C, after which the supernatant was collected by centrifugation and filtered through a 0.22μm pore-size syringe filter. The recombinant protein was purified using a gravity column with Glutathione Sepharose 4B resin (17075601; GE healthcare, Massachusetts) which was washed with the re-suspension buffer 3 times and eluted with PBS, pH 7.5 containing 10mM GSH (G4251-25G, Sigma-Aldrich, Germany) at 4°C. Then, the samples from cell re-suspension, lysate, supernatant, column flow-through, resin wash buffer and resin elution buffer were analyzed by SDS-PAGE to identify the collected protein. The elution fractions were combined and concentrated to 1mL using a 10kD molecular weight cutoff ultracentrifuge tube (UFC901096; Millipore, Germany) and loaded onto a size exclusion chromatography Superdex200 10/300GL column (28-9909-44; GE Healthcare, Massachusetts), which was eluted with PBS, pH 7.4 at room temperature. Fraction size was set to 0.5mL and each fraction was analyzed by SDS-PAGE. The SEC-purified protein was shock-frozen in liquid nitrogen and stored in -80 °C.

His-gH/gL was expressed in HEK-293T cells, which were transfected with the expression plasmid using polyethylenimine (PEI; 23966-1, Polysciences, Pennsylvania) to HEK-293T cells at a ratio of 1mg plasmid/ 5mg PEI / 1×10^6 cells / 1L. The plasmid and PEI were diluted with HEK-293T medium (UP1000, Union, China) to 0.05mg mL^{-1} and 0.25mg mL^{-1} individually and mixed together for 15 minutes at room temperature before adding to adequate amount of cells. The transfected cells were cultured for 7 days under shaking at 120rpm. The supernatant was collected through centrifugation and filtered through a 0.22μm pore-size membrane. The following purification procedures were similar to those for protein expression in *E.coli*. His-resin (88229; Thermo, California) was used for affinity chromatography, washed by PBS pH7.4, 30mM imidazole (1460GR500; Biofroxx, Germany) and eluted by PBS pH7.4 (ZLI-9062; OriGene, China), 300mM imidazole. During SEC, PBS pH7.4 was used as running buffer for SEC.

Immunoprecipitation and GST pull-down assay. For the co-immunoprecipitation assay, HEK-293T cells were transfected with the indicated plasmid and lysed in lysis buffer containing 1%NP-40 (N885726; Macklin, China), 150mM NaCl (13423-6X1KG-R; Invitrogen, California), 2.5mM EDTA (E6758; Sigma-Aldrich, Germany), 20mM HEPES (H7523; Sigma-Aldrich, Germany) pH7.4 and protease inhibitor cocktail at 36h post transfection. The lysates were cleared by centrifugation at 12000 rpm and 4°C 10min . The supernatants were incubated with ANTI-FLAG M2 Gel (A2220, Sigma-Aldrich, Germany) or Anti-c-Myc Agarose Affinity Gel (A7470, Sigma-Aldrich, Germany) overnight. Then, the gels with bound protein were washed three times with lysis buffer and subjected to WB analysis. For the GST pull-down assay, GST-R9AP$^{1-210}$ and His-gH/gL were incubated in lysis buffer overnight, then washed three times with lysis buffer and analyzed by WB. For the antibody competition binding assay, HEK-293T cells were transfected with plasmids encoding FLAG-R9AP or Myc-gH/gL for 36h, and lysed in lysis buffer. HEK-293T cells transfected with empty vector were used as control. Lysates containing Myc-gH/gL protein were incubated with 5mg IgG control, 5mg Ammo1, 10mg Ammo1, 5mg CL59 or 10mg CL59 overnight, and then incubated with lysates containing FLAG-R9AP or the control overnight. Finally, Myc-gH/gL was pulled down using Anti-c-Myc Agarose Affinity Gel which was then washed three times with lysis buffer and subjected to WB analysis.

Biolayer Interferometry (BLI). BLI assays were performed on an Octet Red 96 instrument (18-1127; ForteBio, California) at 30°C with shaking at 1000rpm. All signals were recorded at standard frequency (5.0Hz). For kinetic analysis, Ni-NTA biosensors (18-5101; ForteBio, California) were incubated in PBS with 0.05% Tween20 (P7949; Sigma-Aldrich, Germany), the dilution buffer used throughout the whole assay, for 15min before performing the kinetic analysis. After 60s of primary baseline, His-gH/gL protein diluted with the buffer was loaded at 0.5mg mL^{-1} for 120s, followed by a secondary baseline equilibration for 30s. Then, the association of baseline-control and GST-R9AP$^{1-210}$ at a gradient of concentration from 6.25nM to 100nM was recorded for 180s, followed by a transition to a dissociation process for 600s and multiple rounds of regeneration with 10mM Glycine pH1.5 (GE healthcare). Similar procedures were performed for determination of binding affinity of R9AP peptide/control peptide to gH/gL, except changes of association time and dissociation time to 100s and 200s.The raw curves were baseline-subtracted before fitting to the 1:1 binding model using the ForteBio data analysis software, after which the mean kinetic parameters (kD, kon, koff etc.) were rendered via a global fit to all binding curves. For competition analysis, His-gH/gL protein diluted with the same buffer was loaded onto the Ni-NTA biosensor at 1μg mL^{-1} for 180s. After 30s of equilibration, primary association of R9AP or PBST was recorded until saturation for 600s, followed by the secondary association of AMMO1 or CL59 for another 600s. The concentrations of GST-R9AP$^{1-210}$, AMMO1 antibody and CL59 antibody used in the assay were 200nM, 100nM, and 100nM, respectively. The sensors were regenerated with 10mM Glycine pH1.5. Real-time binding was recorded during the experiment and competitive/non-competitive behavior was determined by the binding response presented by different association couples.

Immunofluorescence staining. For the co-localization assay of R9AP with Alexa Flour 594-labelled EBV, HNE1 cells were transfected with a plasmid expressing eGFP-tagged R9AP for 24h, then co-incubated with EBV labeled with Alexa Fluor 594 (R37117, Molecular Probes, California) for 1h at 37°C. After removing the unbound virus, cells were fixed with 4% paraformaldehyde (N1012, NCM biotech, China) in PBS for 20min at room temperature, and permeabilized with 0.1% Triton X-100 (0219485480; MPbio, California). The cell nuclei were counter-stained with 0.1% DAPI (D9542; Sigma-Aldrich, Germany). For the determination of exogenous R9AP localization, HNE1 cells were transfected with the indicated plasmids for 36h, then fixed with 4% paraformaldehyde in PBS, and either permeabilized with 0.1% Triton X-100 or left untreated. Then, the cells were incubated with an antibody specific for the Myc tag (M5546; Sigma-Aldrich, Germany) and an Alexa Flour 594-labelled goat anti-mouse IgG antibody. The cell nuclei were counter-stained with 0.1% DAPI. To detect the endogenous R9AP localization, HNE1 cells were fixed with 4% paraformaldehyde in PBS and incubated with an antibody targeting R9AP (HPA049791, Sigma-Aldrich, diluted 1:100) and Alexa Flour 594-labelled goat anti-mouse IgG antibody. The cell nuclei were counter-stained with 0.1% DAPI.

PSP digestion assay. Cells in 12-well plates were transfected with the indicated plasmids for 24h, and then fixed in 4% paraformaldehyde. Then, 10μg PSP was diluted in 500μl PBS and incubated with the fixed cells at 4°C for 8 h. The treated cells were washed three times with PBS and collected for WB analysis.

In vivo **EBV infection of humanized mice.** Ten immunodeficient B-NDG mice were purchased from BIOCYTOGEN (China), and divided into two groups. Human cord blood was obtained from Guangzhou Women and Children's Medical Center (China) after obtaining informed consent. Human cord blood mononuclear cells were separated using Ficoll-Hypaque density gradient, and then 1×10^7 cells were injected i.p. into 4 to 5-week-old B-NDG mice. At the same day, mice were injected through the tail vein with $R9AP^{19-30}$ peptide or control peptide at 20mg/kg of body weight, together with 30,000 infectious EBV particles. Then, the mice were injected intraperitoneally with $R9AP^{19-30}$ peptide or control peptide at 20mg/kg of body weight on days -3, -7 and -14, and injected intraperitoneally with 50 mg OKT3 (B104; Nobimpex, Germany) on day -7. Blood was collected from the mice to extract DNA from mice on days- 0, -14, -28 and -42.

Measurement of EBV titers in mouse blood. To quantify the EBV DNA copy number in mouse blood, qPCR was used to detect the BamHI-W fragment of the EBV genome using the primers 5'-CCCAACACTCCACCACACC-3' and 5'-TCTTAGGAGCTGTCCGAGGG-3'. A calibration curve was made based on the EBV Nucleic Acid standards (BDS).

Analysis of R9AP and EBERs expression in human tissues. Samples of human tissue from the tongue, floor of the mouth, lymphoid tissuse, nasopharyngeal carcinoma, gastric carcinoma and B cell lymphoma were all obtained from patients who were admitted to the Sun Yat-sen University Cancer Center, and signed written informed consent forms. Samples of tissue from the tongue, floor of the mouth, and lymphoid tissues were analyzed by hematoxylin-eosin staining (H□E) and R9AP antibody staining. To detect R9AP, the rabbit polyclonal antibody against human R9AP (HPA049791, Sigma-Aldrich, diluted 1:50) was used as primary antibodies, which was incubated overnight at 4°C. After washing three times in PBST, the tissue sections were incubated with anti-rabbit secondary antibody (1:1000, Zymed, California), and then treated with 3-diaminobenzidine tetrahydrochloride for 10 seconds, followed by staining with 10% Mayer's hematoxylin (ZSGB-Bio). Staining of paraffin-embedded tissue sections for EBV EBERs was performed using the ISH detection Kit (ISH-7001, ZSGB-Bio, China).

Analysis of the spleen of EBV-infected mice. After the death of all the ctrl-treated mice, the $R9AP^{19-30}$-treated mice were euthanized. The spleens of all the mice were fixed in formalin to examine if the animals had persistent EBV infection using H□E staining, IHC staining with antibodies against human CD20 (B cell marker), and detection of EBV EBERs using the ISH detection Kit. The results were independently evaluated by two pathologists, who were blinded to the status of the samples. The expression of human CD20 and EBV EBERs was evaluated by counting 3 representative high-power fields (×40 objective) per sample, with approximately 100 to 200 cells/field. The proportion of EBER-positive cells compared to human CD20-positive cells in the spleens of EBV infected humanized B-NDG mice was then calculated.

Plasmids. For EBV infection of HEK-293T or epithelial cells, cDNA fragments encoding R9AP, SLC26A9, CNGA1, the N-terminal amino acids 1 to 210 of R9AP (1-210), N-terminal plus transmembrane domain of R9AP (1-231), deletion of amino acids 1 to 50 of R9AP (△1-50), deletion of amino acids 51 to 100 of R9AP (△51-100), deletion of amino acids 101 to 152 of R9AP (△101-152) and deletion of amino acids 153 to 200 of R9AP (△153-200) were individually cloned into PCDNA3.1 (+) vector (V79020, Invitrogen, California); for EBV infection of EBV-negative Akata cells, the cDNA fragment encoding R9AP was cloned into the pBABE-Puro retroviral vector (Cell Biolabs, RTV-001-puro, California); for immunofluorescence staining in HNE1 cells, the cDNA of full-length of R9AP ($R9AP^{FL}$) or N-terminal amino acids 1 to 210 of R9AP ($R9AP^{1-210}$) was cloned into the pCDNA6-Myc vector (V221-20, Invitrogen, California); for the PSP digestion assay, the sequence encoding the PSP recognition site and full-length sequence of R9AP (psp-$R9AP^{FL}$) or PSP site and N-terminal amino acids 1 to 210 of R9AP (psp-$R9AP^{1-210}$) were cloned into the pCDNA3.1 (+) vector; for the immunoprecipitation assay, cDNA of R9AP was cloned into pCDNA3.1 (+) vector, myc-gH, gL or myc-gB were cloned into the pCDNA6-Myc vector; for the GST pull-down assay and protein expression, the sequence encoding N-terminal amino acids 1 to 210 R9AP was cloned into the

pGEX6p-1-GST vector, which was a kind gift from Professor Song Gao (Sun Yat-sen University Cancer Center), and the sequences of gL (23-137AA, M81 strain) and gH ectodomain (19-679AA, M81 strain) connected by a linker (GGGGS)x3 were cloned into the pCDNA3.1(+) vector; for the cell-based fusion assay, expression plasmids for pCAG-T7, pT7EMC-Luc, gB, gH or gL, which were a kind gift from Wolfgang Hammerschmidt (Helmholtz Zentrum Munich) and Professor R. Longnecker (Northwestern University), were used.

Quantitative real-time PCR. Total RNA was extracted using TRIzol reagent (T9424; Sigma-Aldrich, Germany). To analyze gene expression, 1μg of RNA was reverse-transcribed using the RNA Reverse Transcription System (A5001; Promega, Wisconsin). The mRNA level was quantified using the LightCycler 480 SYBR Green I Master mix (04887352001; Roche, Switzerland) on a Roche LightCycler 480 instrument. All the gene expression data were normalized to the housekeeping gene beta actin (ACTB). Primers are listed below:

CNGA1: 5’-AAGGGAGGACCATCACAGA-3’ and 5’-TTCTGGTTCCTGGTCCTTA-3’

GPR1: 5’-TCTTATCTCATCGGCATCG-3’ and 5’-GCTTCGCTTCTTCACCTT -3’

SLC26A9:5’-CAACAAGCACGGCTACGAC-3’ and 5’-TTGAGGGAGTTCTTGAGATTGA-3’

R9AP: 5’-ATGAAGAGCGTTCGTGCCG-3’ and 5’-GCACGCAGTCGTCTTGTTGAG-3’

Statistical analyses. The results represent the means ± SEM from three independent experiments. The two-tailed unpaired Student’s *t*-test was used for statistical analysis involving two group comparisons for all *in vitro* experiments and detection of EBV DNA copy numbers in mice at the 6^{th} week (ns, not significant; *P< 0.05, **P< 0.01, ***P< 0.001). A Log-rank test was used for statistical analysis involving two group comparisons for survival in the *in vivo* experiments. Statistical analyses were performed using GraphPad Prism (GraphPad Software, San Diego, CA).

Ethical standards. Written informed consents forms were signed by all the patients. All the utilization of human samples was approved by the institutional review board of each institution taking part in the project. All animal experiments with infectious EBV were performed in the animal biosafety level 2 facilities at Sun Yat-sen University Zhongshan School of Medicine, which was approved by the Committee on the Ethics of Animal Experiments of Sun Yat-sen University. The animal studies were carried out in strict accordance with the recommendations promulgated in the Guide for the Care and Use of Laboratory Animals of the Ministry of Science and Technology of the People’s Republic of China.

References

1. Fleisher, G., Henle, W., Henle, G., Lennette, E. T. & Biggar, R. J. Primary infection with Epstein-Barr virus in infants in the United States: clinical and serologic observations. *The Journal of infectious diseases* **139**, 553–558, doi:10.1093/infdis/139.5.553 (1979).
2. Luzuriaga, K. & Sullivan, J. L. Infectious mononucleosis. *The New England journal of medicine* **362**, 1993–2000, doi:10.1056/NEJMcp1001116 (2010).
3. Odumade, O. A., Hogquist, K. A. & Balfour, H. H., Jr. Progress and problems in understanding and managing primary Epstein-Barr virus infections. *Clin Microbiol Rev* **24**, 193–209, doi:10.1128/CMR.00044-10 (2011).
4. Fernandez-Menendez, S., Fernandez-Moran, M., Fernandez-Vega, I., Perez-Alvarez, A. & Villafani-Echazu, J. Epstein-Barr virus and multiple sclerosis. From evidence to therapeutic strategies. *Journal of the neurological sciences* **361**, 213–219, doi:10.1016/j.jns.2016.01.013 (2016).
5. Pender, M. P. The essential role of Epstein-Barr virus in the pathogenesis of multiple sclerosis. *Neuroscientist* **17**, 351–367, doi:10.1177/1073858410381531 (2011).
6. Bar-Or, A. *et al.* Epstein-Barr Virus in Multiple Sclerosis: Theory and Emerging Immunotherapies. *Trends Mol Med* **26**, 296–310, doi:10.1016/j.molmed.2019.11.003 (2020).
7. Tan, R. *et al.* Clinical utility of Epstein-Barr virus DNA and other liquid biopsy markers in nasopharyngeal carcinoma. *Cancer Commun (Lond)*, doi:10.1002/cac2.12100 (2020).
8. Epstein, M. A., Achong, B. G. & Barr, Y. M. Virus Particles in Cultured Lymphoblasts from Burkitt's Lymphoma. *Lancet* **1**, 702–703, doi:10.1016/s0140-6736(64)91524-7 (1964).
9. Shannon-Lowe, C. & Rickinson, A. The Global Landscape of EBV-Associated Tumors. *Frontiers in oncology* **9**, 713, doi:10.3389/fonc.2019.00713 (2019).
10. van Zyl, D. G., Mautner, J. & Delecluse, H. J. Progress in EBV Vaccines. *Frontiers in oncology* **9**, 104, doi:10.3389/fonc.2019.00104 (2019).
11. Hutt-Fletcher, L. M. Epstein-Barr virus entry. *Journal of virology* **81**, 7825–7832, doi:10.1128/JVI.00445-07 (2007).
12. Nemerow, G. R., Mold, C., Schwend, V. K., Tollefson, V. & Cooper, N. R. Identification of gp350 as the viral glycoprotein mediating attachment of Epstein-Barr virus (EBV) to the EBV/C3d receptor of B cells: sequence homology of gp350 and C3 complement fragment C3d. *Journal of virology* **61**, 1416–1420 (1987).
13. Ogembo, J. G. *et al.* Human complement receptor type 1/CD35 is an Epstein-Barr Virus receptor. *Cell reports* **3**, 371–385, doi:10.1016/j.celrep.2013.01.023 (2013).
14. Smith, N. A., Coleman, C. B., Gewurz, B. E. & Rochford, R. CD21 (Complement Receptor 2) Is the Receptor for Epstein-Barr Virus Entry into T Cells. *Journal of virology* **94**, doi:10.1128/JVI.00428-20 (2020).
15. Cairns, T. M. *et al.* Capturing the herpes simplex virus core fusion complex (gB-gH/gL) in an acidic environment. *Journal of virology* **85**, 6175–6184, doi:10.1128/JVI.00119-11 (2011).

16. Knox, P. G. & Young, L. S. Epstein-Barr virus infection of CR2-transfected epithelial cells reveals the presence of MHC class II on the virion. *Virology* **213**, 147–157, doi:10.1006/viro.1995.1555 (1995).
17. Mullen, M. M., Haan, K. M., Longnecker, R. & Jardetzky, T. S. Structure of the Epstein-Barr virus gp42 protein bound to the MHC class II receptor HLA-DR1. *Molecular cell* **9**, 375–385, doi:10.1016/s1097-2765(02)00465-3 (2002).
18. Birkenbach, M., Tong, X., Bradbury, L. E., Tedder, T. F. & Kieff, E. Characterization of an Epstein-Barr virus receptor on human epithelial cells. *The Journal of experimental medicine* **176**, 1405–1414, doi:10.1084/jem.176.5.1405 (1992).
19. Yoshiyama, H., Imai, S., Shimizu, N. & Takada, K. Epstein-Barr virus infection of human gastric carcinoma cells: implication of the existence of a new virus receptor different from CD21. *Journal of virology* **71**, 5688–5691 (1997).
20. Wang, X., Kenyon, W. J., Li, Q., Mullberg, J. & Hutt-Fletcher, L. M. Epstein-Barr virus uses different complexes of glycoproteins gH and gL to infect B lymphocytes and epithelial cells. *Journal of virology* **72**, 5552–5558 (1998).
21. Janz, A. *et al.* Infectious Epstein-Barr virus lacking major glycoprotein BLLF1 (gp350/220) demonstrates the existence of additional viral ligands. *Journal of virology* **74**, 10142–10152, doi:10.1128/jvi.74.21.10142-10152.2000 (2000).
22. Wang, X. & Hutt-Fletcher, L. M. Epstein-Barr virus lacking glycoprotein gp42 can bind to B cells but is not able to infect. *Journal of virology* **72**, 158–163, doi:10.1128/JVI.72.1.158-163.1998 (1998).
23. Tugizov, S. M., Berline, J. W. & Palefsky, J. M. Epstein-Barr virus infection of polarized tongue and nasopharyngeal epithelial cells. *Nature medicine* **9**, 307–314, doi:10.1038/nm830 (2003).
24. Chesnokova, L. S., Nishimura, S. L. & Hutt-Fletcher, L. M. Fusion of epithelial cells by Epstein-Barr virus proteins is triggered by binding of viral glycoproteins gHgL to integrins alphavbeta6 or alphavbeta8. *Proceedings of the National Academy of Sciences of the United States of America* **106**, 20464–20469, doi:10.1073/pnas.0907508106 (2009).
25. Chesnokova, L. S. & Hutt-Fletcher, L. M. Fusion of Epstein-Barr virus with epithelial cells can be triggered by alphavbeta5 in addition to alphavbeta6 and alphavbeta8, and integrin binding triggers a conformational change in glycoproteins gHgL. *Journal of virology* **85**, 13214–13223, doi:10.1128/JVI.05580-11 (2011).
26. Song, L. B. *et al.* Bmi-1 is a novel molecular marker of nasopharyngeal carcinoma progression and immortalizes primary human nasopharyngeal epithelial cells. *Cancer research* **66**, 6225–6232, doi:10.1158/0008-5472.CAN-06-0094 (2006).
27. Xiong, D. *et al.* Nonmuscle myosin heavy chain IIA mediates Epstein-Barr virus infection of nasopharyngeal epithelial cells. *Proceedings of the National Academy of Sciences of the United States of America* **112**, 11036–11041, doi:10.1073/pnas.1513359112 (2015).
28. Wang, H. B. *et al.* Neuropilin 1 is an entry factor that promotes EBV infection of nasopharyngeal epithelial cells. *Nature communications* **6**, 6240, doi:10.1038/ncomms7240 (2015).

29. Chen, J. *et al.* Ephrin receptor A2 is a functional entry receptor for Epstein-Barr virus. *Nature microbiology*, doi:10.1038/s41564-017-0081-7 (2018).
30. Zhang, H. *et al.* Ephrin receptor A2 is an epithelial cell receptor for Epstein-Barr virus entry. *Nature microbiology*, doi:10.1038/s41564-017-0080-8 (2018).
31. Connolly, S. A., Jackson, J. O., Jardetzky, T. S. & Longnecker, R. Fusing structure and function: a structural view of the herpesvirus entry machinery. *Nature reviews. Microbiology* **9**, 369–381, doi:10.1038/nrmicro2548 (2011).
32. Matsuura, H., Kirschner, A. N., Longnecker, R. & Jardetzky, T. S. Crystal structure of the Epstein-Barr virus (EBV) glycoprotein H/glycoprotein L (gH/gL) complex. *Proceedings of the National Academy of Sciences of the United States of America* **107**, 22641–22646, doi:10.1073/pnas.1011806108 (2010).
33. Chowdary, T. K. *et al.* Crystal structure of the conserved herpesvirus fusion regulator complex gH-gL. *Nature structural & molecular biology* **17**, 882–888, doi:10.1038/nsmb.1837 (2010).
34. Snijder, J. *et al.* An Antibody Targeting the Fusion Machinery Neutralizes Dual-Tropic Infection and Defines a Site of Vulnerability on Epstein-Barr Virus. *Immunity* **48**, 799–811 e799, doi:10.1016/j.immuni.2018.03.026 (2018).
35. Singh, S. *et al.* Neutralizing Antibodies Protect against Oral Transmission of Lymphocryptovirus. *Cell Rep Med* **1**, doi:10.1016/j.xcrm.2020.100033 (2020).
36. Speck, P. & Longnecker, R. Epstein-Barr virus (EBV) infection visualized by EGFP expression demonstrates dependence on known mediators of EBV entry. *Archives of virology* **144**, 1123–1137, doi:10.1007/s007050050574 (1999).
37. Sathiyamoorthy, K. *et al.* Inhibition of EBV-mediated membrane fusion by anti-gHgL antibodies. *Proceedings of the National Academy of Sciences of the United States of America* **114**, E8703-E8710, doi:10.1073/pnas.1704661114 (2017).
38. Hu, G. & Wensel, T. G. R9AP, a membrane anchor for the photoreceptor GTPase accelerating protein, RGS9-1. *Proceedings of the National Academy of Sciences of the United States of America* **99**, 9755–9760, doi:10.1073/pnas.152094799 (2002).
39. UniProt Consortium, T. UniProt: the universal protein knowledgebase. *Nucleic acids research* **46**, 2699, doi:10.1093/nar/gky092 (2018).
40. Pearring, J. N., Lieu, E. C., Winter, J. R., Baker, S. A. & Arshavsky, V. Y. R9AP targeting to rod outer segments is independent of rhodopsin and is guided by the SNARE homology domain. *Molecular biology of the cell* **25**, 2644–2649, doi:10.1091/mbc.E14-02-0747 (2014).
41. Mitchell, A. L. *et al.* InterPro in 2019: improving coverage, classification and access to protein sequence annotations. *Nucleic acids research* **47**, D351-D360, doi:10.1093/nar/gky1100 (2019).
42. Krogh, A., Larsson, B., von Heijne, G. & Sonnhammer, E. L. Predicting transmembrane protein topology with a hidden Markov model: application to complete genomes. *Journal of molecular biology* **305**, 567–580, doi:10.1006/jmbi.2000.4315 (2001).
43. Cannon, M. J., Pisa, P., Fox, R. I. & Cooper, N. R. Epstein-Barr virus induces aggressive lymphoproliferative disorders of human B cell origin in SCID/hu chimeric mice. *The Journal of*

clinical investigation **85**, 1333–1337, doi:10.1172/JCI114573 (1990).

44. Haque, T. *et al.* A mouse monoclonal antibody against Epstein-Barr virus envelope glycoprotein 350 prevents infection both in vitro and in vivo. *The Journal of infectious diseases* **194**, 584–587, doi:10.1086/505912 (2006).
45. Ma, S. D. *et al.* LMP1-deficient Epstein-Barr virus mutant requires T cells for lymphomagenesis. *The Journal of clinical investigation* **125**, 304–315, doi:10.1172/JCI76357 (2015).
46. Ma, S. D. *et al.* PD-1/CTLA-4 Blockade Inhibits Epstein-Barr Virus-Induced Lymphoma Growth in a Cord Blood Humanized-Mouse Model. *PLoS pathogens* **12**, e1005642, doi:10.1371/journal.ppat.1005642 (2016).
47. Young, L. S. & Rickinson, A. B. Epstein-Barr virus: 40 years on. *Nature reviews. Cancer* **4**, 757–768, doi:10.1038/nrc1452 (2004).
48. Wang, Y. *et al.* Novel Biomarkers Associated With Progression and Prognosis of Bladder Cancer Identified by Co-expression Analysis. *Frontiers in oncology* **9**, 1030, doi:10.3389/fonc.2019.01030 (2019).
49. Young, L. S., Yap, L. F. & Murray, P. G. Epstein-Barr virus: more than 50 years old and still providing surprises. *Nature reviews. Cancer*, doi:10.1038/nrc.2016.92 (2016).
50. Molesworth, S. J., Lake, C. M., Borza, C. M., Turk, S. M. & Hutt-Fletcher, L. M. Epstein-Barr virus gH is essential for penetration of B cells but also plays a role in attachment of virus to epithelial cells. *Journal of virology* **74**, 6324–6332, doi:Doi 10.1128/Jvi.74.14.6324–6332.2000 (2000).
51. Hanto, D. W., Sakamoto, K., Purtilo, D. T., Simmons, R. L. & Najarian, J. S. The Epstein-Barr virus in the pathogenesis of posttransplant lymphoproliferative disorders. Clinical, pathologic, and virologic correlation. *Surgery* **90**, 204–213 (1981).
52. Rea, D. *et al.* Epstein-Barr virus latent and replicative gene expression in post-transplant lymphoproliferative disorders and AIDS-related non-Hodgkin's lymphomas. French Study Group of Pathology for HIV-associated Tumors. *Annals of oncology: official journal of the European Society for Medical Oncology* **5 Suppl 1**, 113–116, doi:10.1093/annonc/5.suppl_1.s113 (1994).
53. List, A. F., Greco, F. A. & Vogler, L. B. Lymphoproliferative diseases in immunocompromised hosts: the role of Epstein-Barr virus. *Journal of clinical oncology: official journal of the American Society of Clinical Oncology* **5**, 1673–1689, doi:10.1200/JCO.1987.5.10.1673 (1987).
54. Messick, T. E. *et al.* Structure-based design of small-molecule inhibitors of EBNA1 DNA binding blocks Epstein-Barr virus latent infection and tumor growth. *Science translational medicine* **11**, doi:10.1126/scitranslmed.aau5612 (2019).
55. Jiang, L. *et al.* EBNA1-targeted inhibitors: Novel approaches for the treatment of Epstein-Barr virus-associated cancers. *Theranostics* **8**, 5307–5319, doi:10.7150/thno.26823 (2018).
56. Michaelides, M. *et al.* Novel mutations and electrophysiologic findings in RGS9- and R9AP-associated retinal dysfunction (Bradyopsia). *Ophthalmology* **117**, 120–127 e121, doi:10.1016/j.ophtha.2009.06.011 (2010).

57. Strauss, R. W. *et al.* Retinal Architecture in RGS9- and R9AP-Associated Retinal Dysfunction (Bradyopsia). *Am J Ophthalmol* **160**, 1269–1275 e1261, doi:10.1016/j.ajo.2015.08.032 (2015).

Declarations

Acknowledgments: We thank Dr. Maria Masucci (Karolinska Institute, Sweden) for providing the EBV-positive Akata cell line, Dr. Quen-Tin Liu (Sun Yat-sen University, Guangzhou, China) for providing the CNE1 cell line, Dr. Sai-Wah Tsao (University of Hong Kong, Hong Kong SAR) for providing the HNE1 and HK1 cell lines, Dr. Qian Tao (Chinese university of Hong Kong, Hong Kong SAR) for providing the AGS cell line, Dr. Xu Rui-Hua (Sun Yat-sen University, Guangzhou, China) for providing the MKN74 cell line, Dr. Jia-Huai Han (XIAMEN University, Fujian, People's Republic of China) for providing the SLC26A9 cDNA, Dr. Richard Longnecker and Dr. Patricia G. Spear (Northwestern University) for providing plasmids pCAGT7 and pT7EMCLuc, as well as CL59 antibody, Dr. Wolfgang Hammerschmidt (Helmholtz Zentrum München) for providing Plasmid p2670, and finally the two pathologists, Dr. Yu-Hua Huang and Dr. Yu Zhang (Sun Yat-sen University, Guangzhou, China), for the evaluation of immunostaining and EBERs in situ hybridization of human and mouse samples. This manuscript was edited at Life Science Editors.

Funding: This work was supported by the National Key Research and development program of China (2016YFA0502101, 2017YFA0505600) and the National Natural Science Foundation of China (81520108022, 81621004, 81802729, 81872224).

Author contributions: Mu-Sheng Zeng conceived and designed the experiments, provided supervision and wrote the manuscript. Yan Li performed and analyzed the key experiments and wrote the manuscript. Hua Zhang, Xiao-Dong Dong and Cong Sun performed and analyzed the key experiments. Xiang-Wei Kong, Dan-Ling Dai, Qian-Ying Zhu, Li Yuan and Yu-Chun Li performed the experiments. Qian Zhong, Andrew T. McGuire, Bo Zhao and Yi-Xin Zeng provided constructive suggestions for this work. Bo Zhao and Andrew T. McGuire helped to revise the manuscript.

Competing interests: The authors declare no competing financial interests.

Figures

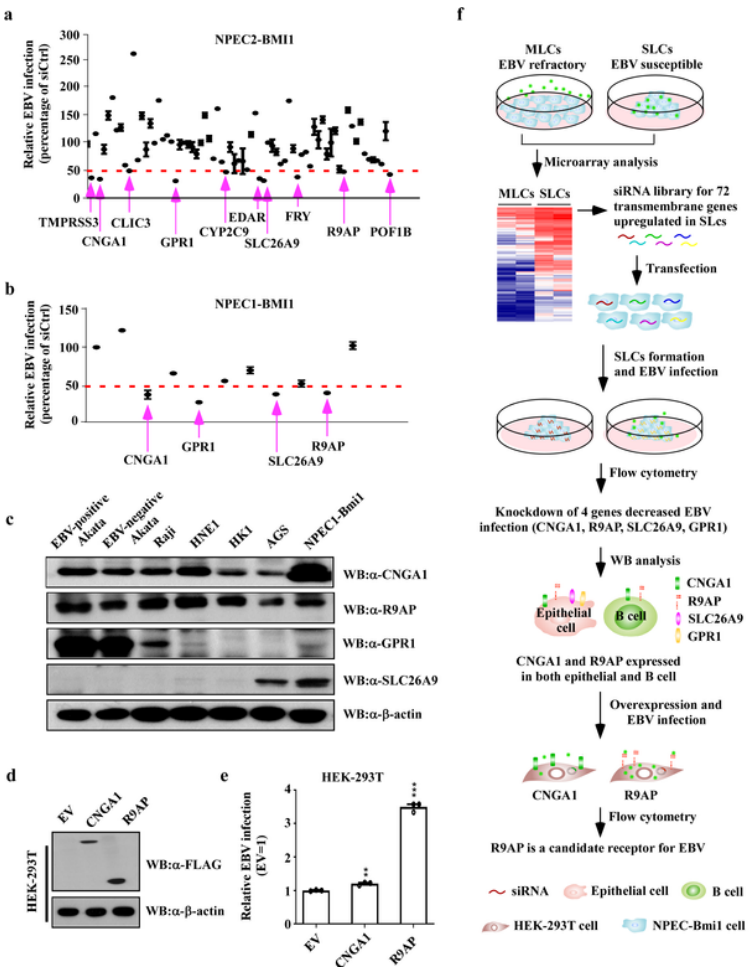

Figure 1

Identification of R9AP as a potential EBV receptor in both epithelial cells and B cells. a, b, siRNA screening. Relative EBV infection efficiency of NPEC-Bmi SLCs transfected with siRNA pools was determined by flow cytometry. 72 siRNA pools were screened in NPEC2-Bmi1 SLCs firstly (a), and 10 siRNA pools were selected and re-screened in NPEC1- Bmi1 SLCs (b). siCtrl, negative control siRNA. Arrows indicate that knockdown of individual gene by siRNA pool reduced EBV infection efficiency more than fifty percent compared to the siCtrl. The dotted pink line indicate 50% of relative EBV infected cells in siCtrl transfected SLCs. The mean value of siCtrl was normalized to 100%. Results are expressed as mean ± s.e.m. from two independent experiments. c, Western blotting (WB) analysis of endogenous CNGA1, R9AP, GPR-1 and SLC26A9 in EBV susceptible cells. β-actin was used as loading control. d, HEK-293T cells were harvested 24h after transfection with empty vector (EV) or a vector expressing FLAG-tagged CNGA1 or FLAG-tagged R9AP and analyzed by WB with the indicated antibodies. β-actin was used as loading control. e, HEK-293T cells were infected with EBV at MOI of ≈300 24h after transfection with a vector expressing CNGA1 or R9AP or with EV and analyzed for the infection efficiency by flow cytometry 24h after EBV infection. Bars represent percentage of infection, with the infection efficiency of EV-transfected cells normalized to 1. Results are expressed as mean ± s.e.m. from three independent experiments, two-tailed unpaired Student's t-test (**P < 0.01; ***P < 0.001). f, Schematic representation of the screening. Microarray was used to analyze the altered genes in SLCs compared to MLCs of NPECs. A

siRNA library targeting the upregulated transmembrane genes in SLCs was synthesized and transfected into NPECs. Knocking down CNGA1, R9AP, SLC26A9 or GPR1 reduced EBV infection more than 50% in NPECs. Then endogenous protein expression of CNGA1, R9AP, SLC26A9, or GPR1 in cell lines was analyzed by WB. CNGA1 and R9AP were expressed in all indicated cell lines. Finally, CNGA1 and R9AP plasmids were transfected into HEK-293T cells, and only R9AP enhanced EBV infection remarkably.

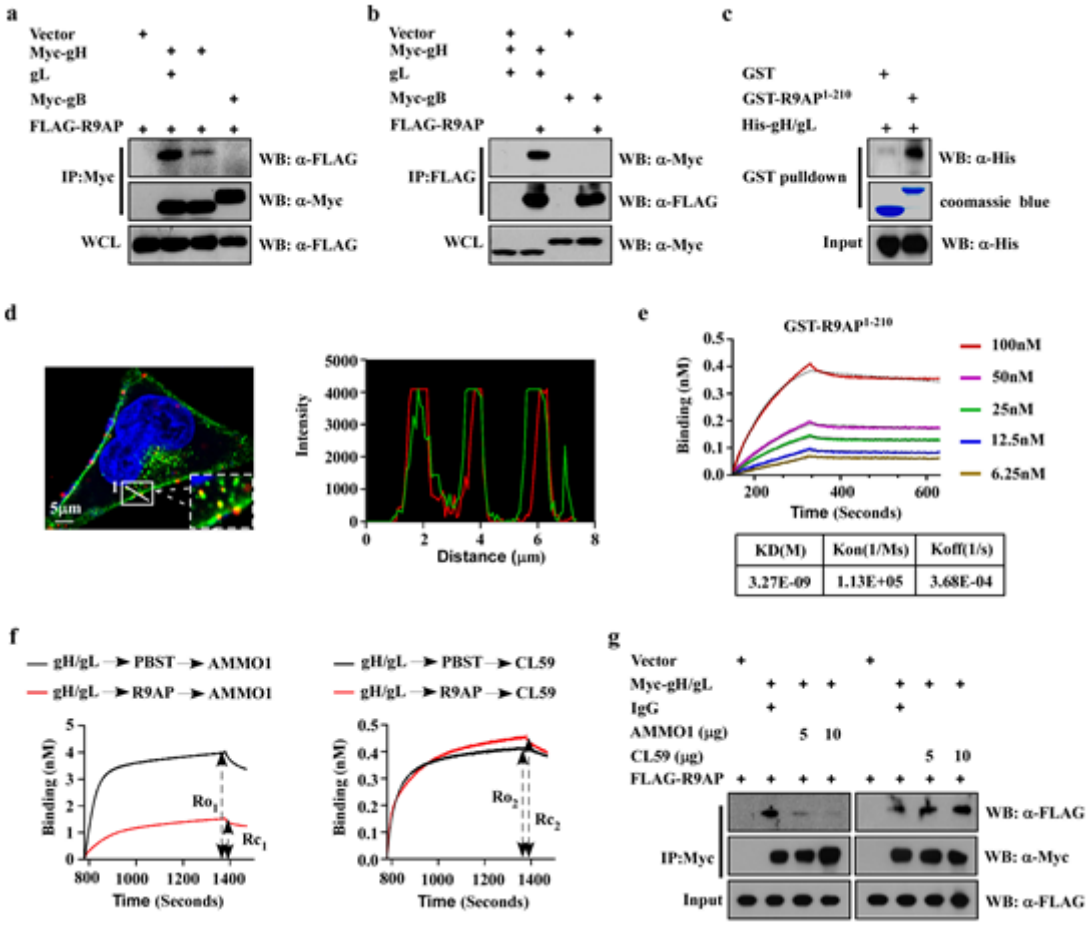

Figure 2

R9AP directly interacts with EBV gH/gL glycoproteins and co-localizes with EBV. a, b, HEK-293T cells were co-transfected with FLAG-R9AP together with EV, Myc-gH and gL, Myc-gH alone, or Myc-gB for 36h, lysed and immunoprecipitated with antibody against Myc (a) or FLAG (b), followed by WB analysis with the indicated antibody. WCL, whole cell lysates. c, Purified His-gH/gL proteins were precipitated with GST or GST-R9AP1-210 proteins and detected by WB using an antibody against the His tag. GST-fusion proteins were detected by coomassie blue staining. d, HNE1 cells were infected with Alexa flour 594-labelled EBV 24h after being transfected with eGFP-R9AP. eGFP-R9AP was visualized as green. Alexa fluor 594-labelled-EBV was imaged as red. Nuclei were stained with DAPI (blue). The numbered inset was shown at higher magnified. Co-localization intensity of the area indicated by the slash was also shown in right panel. e, His-gH/gL proteins were captured onto Ni-NTA biosensors and assayed for binding to GST-R9AP1-210 proteins at the indicated concentrations. Kinetic values calculated from the fit model for binding curves were shown below the graph. f, BLI competition assay of GST-R9AP with antibody

AMMO1 or CL59. The black line represents the binding signal of AMMO1 or CL59 to gH/gL, the red line represents the binding signal of AMMO1 or CL59 to gH/gL after R9AP combining. Rc and Ro represented the response of competitive binding and one ligand binding. The ratio of Rc/Ro reflects the intensity of competition. For the competition of GST-R9AP with antibody AMMO1:Rc1/Ro1= 0.39. For the competition of GST-R9AP with antibody CL59: Rc2/Ro2= 1.02. g, HEK-293T cells were lysed in lysis buffer 36h after transfection with plasmids expressing either FLAG-R9AP or Myc-gH/gL. HEK-293T cells transfected with EV were used as control. Lysates containing Myc-gH/gL protein were pre-incubated with increased amounts of antibody as indicated or an IgG control then incubated with lysates containing FLAG-R9AP overnight. These mixtures were immunoprecipitated with antibody against Myc then WB was performed using the indicated antibodies.

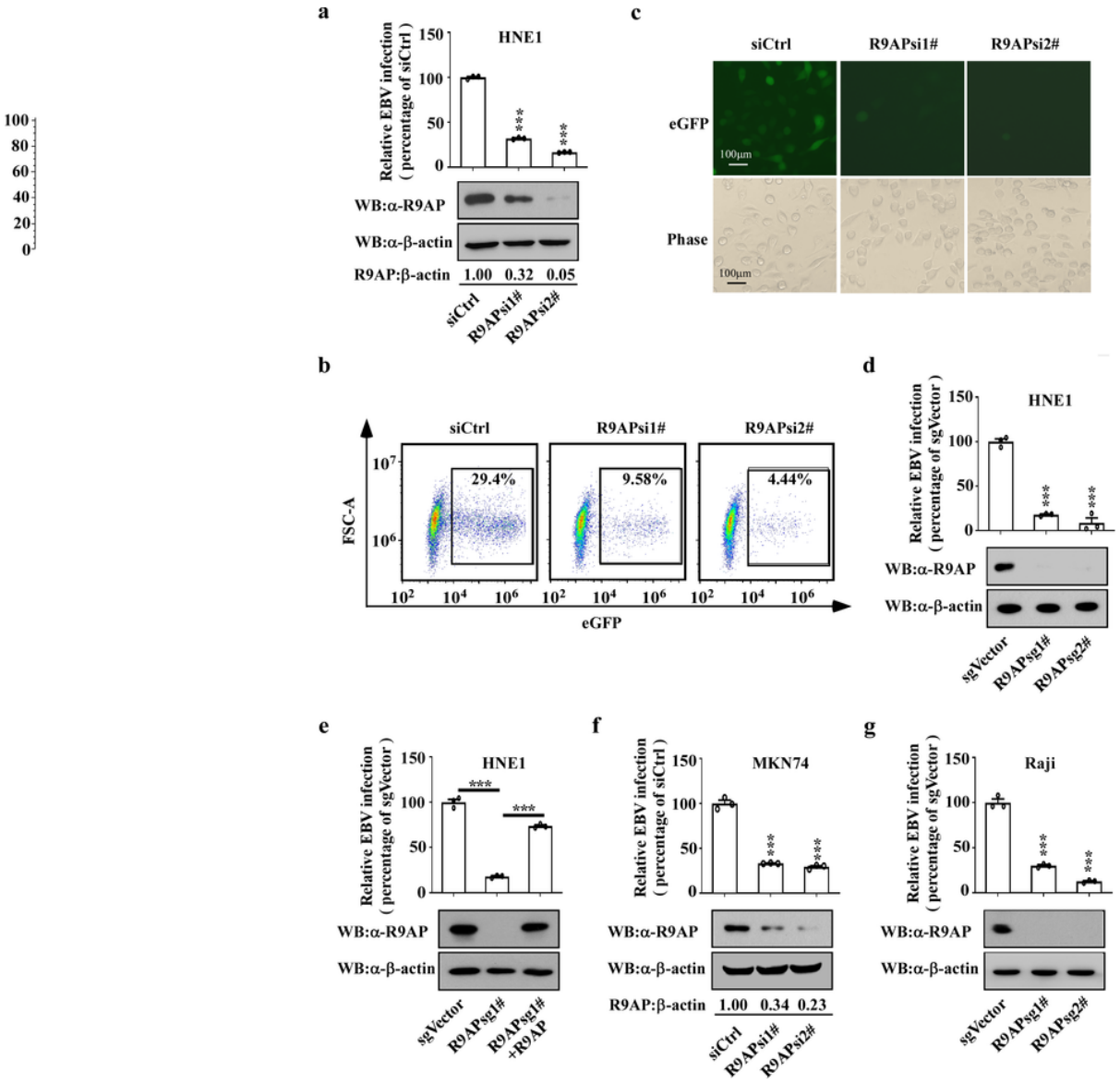

Figure 3

Inhibition of R9AP impairs EBV infection in both epithelial and B cells. a-c, HNE1 cells were transfected with R9AP siRNAs (R9APsi1# or R9APsi2#) or siCtrl for 36h. Some cells were harvested and their R9AP protein level was analyzed by WB (a), using□□-actin as loading control. Remaining cells were infected with

EBV at an MOI of ≈1000 and EBV-positive cells were shown as green in fluorescence images (c). The percentage of infected cells was determined using flow cytometry (b), and the quantification of flow cytometry data from three independent experiments was shown in (a). Bars represent percentage of infection, with infection of siCtrl transfected cells was normalized to 100%. Results are expressed as mean ± s.e.m. from three independent experiments, two-tailed unpaired Student's t-test (***P < 0.001). d, e, The R9AP protein level and EBV infection efficiency in HNE1 cells knockout of R9AP using R9APsg1# and R9APsg2#(d). The empty vector was used as control (sgVector). Then R9AP knockout cells were reconstituted with a R9AP expression vector (R9APsg1# +R9AP) (e).≈≈-actin was used as loading control. EBV at MOI of ≈1000 was added to the R9AP knockout and reconstituted HNE1 cells, and EBV infection efficiency was analyzed by flow cytometry (d, e). Bars represent percentage of infection, with infection of sgVector transfected cells was normalized to 100%. Results are expressed as mean ± s.e.m. from three independent experiments, two-tailed unpaired Student's t-test (***P < 0.001). f, The R9AP protein level and EBV infection efficiency in MKN74 transfected with the indicated siRNA, performed as in (a). Results are expressed as mean ± s.e.m. from three independent experiments, two-tailed unpaired Student's t-test (***P < 0.001). g, The R9AP protein level and EBV infection efficiency in R9AP knockout Raji cells. sgVector, R9APsg1#, or R9APsg2# was delivered into Raji cells by lentivirus package system. Cells were harvested and R9AP protein was analyzed by WB.≈≈-actin was used as loading control. EBV at MOI of ≈1000 was used to infect the R9AP knockout Raji cells and EBV infection efficiency was analyzed by flow cytometry. Bars represent percentage of infection, with infection of sgVector transfected cells was normalized to 100%. Results are expressed as mean ± s.e.m. from three independent experiments, two-tailed unpaired Student's t-test (***P < 0.001).

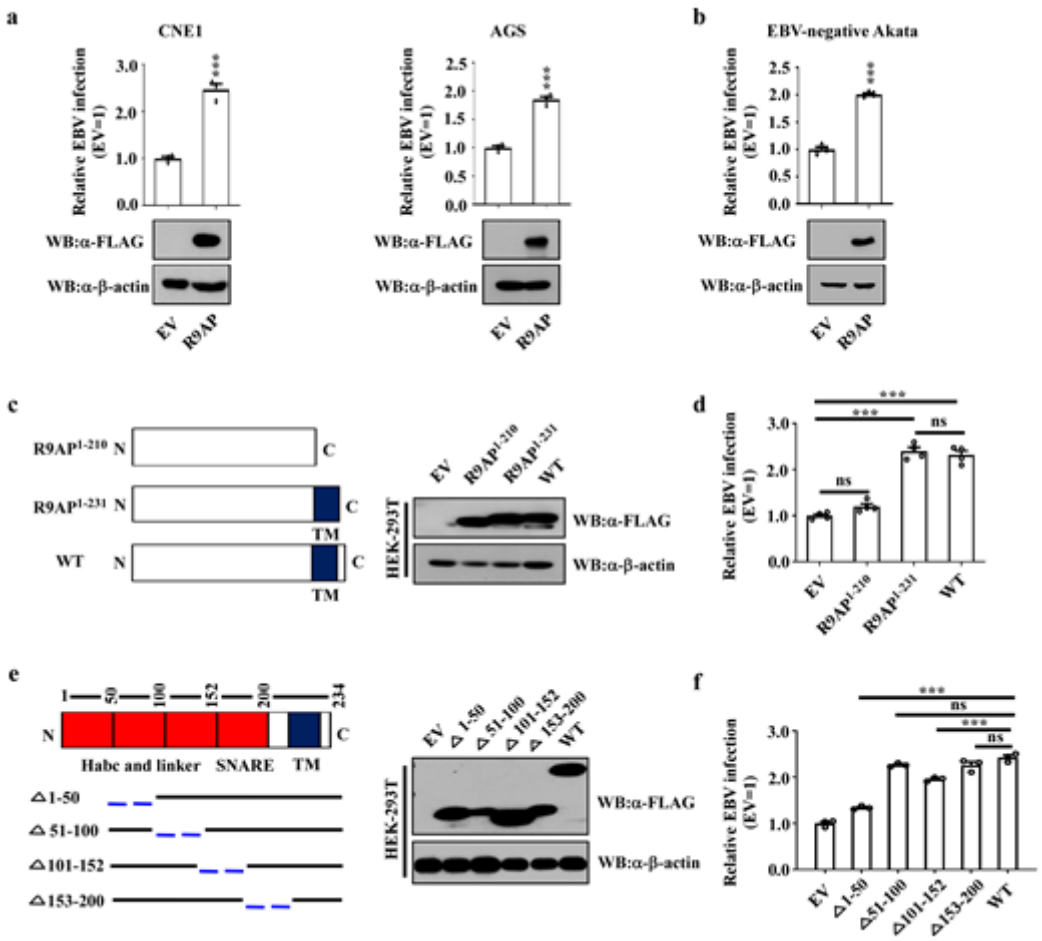

Figure 4

EBV infection depends on the Habc trihelical bundle, linker and transmembrane domain of R9AP. a, b,The protein expression of R9AP and EBV infection efficiency in R9AP overexpressed cells. FLAG tagged R9AP plasmid or EV was transiently transfected into CNE1 cells or AGS cells (a) or stably transfected into EBV-negative Akata cells (b). Cells were harvested and the R9AP expression was analyzed by WB. β-actin was used as loading control. EBV at MOI of 1000 was used to infect these cells and the EBV infection efficiency was analyzed by flow cytometry. Bars represent percentage of infection, with infection of EV transfected cells was normalized to 1. Results are expressed as mean ± s.e.m. from three independent experiments, two-tailed unpaired Student's t-test (***P < 0.001). c, Schematic representation of FLAG tagged R9AP (WT) or truncated mutants R9AP1-210 and R9AP1-231 (left) and their transient expression in HEK-293T cells 36h follow transfection by WB analysis (right). d, Relative EBV infection efficiency in HEK-293T cells expressing indicated ectopic R9AP or R9AP mutants. EBV infection efficiency was analyzed by flow cytometry. Bars represent percentage of infection, with infection of EV transfected cells was normalized to 1. Results are expressed as mean ± s.e.m. from three independent experiments, two-tailed unpaired Student's t-test (ns, not significant; ***P < 0.001). e, Schematic representation of R9AP mutants deleted of amino acids 1-50 (△1-50), amino acids 51-100 (△51-100), amino acids 101-152 (△101-152), or amino acids 153-200 a (△153-200) (left) and expression of these mutants and WT in

HEK-293T cells 36h after transient transfection by WB analysis (right). EV was used as an expression control and-actin was used as loading control. f, Relative EBV infection efficiency in HEK-293T cells expressing indicated ectopic R9AP or R9AP mutants as in (d). Bars represent percentage of infection, with infection of EV transfected cells was normalized to 1. Results are expressed as mean ± s.e.m. from three independent experiments, two-tailed unpaired Student's t-test (ns, not significant; ***P < 0.001).

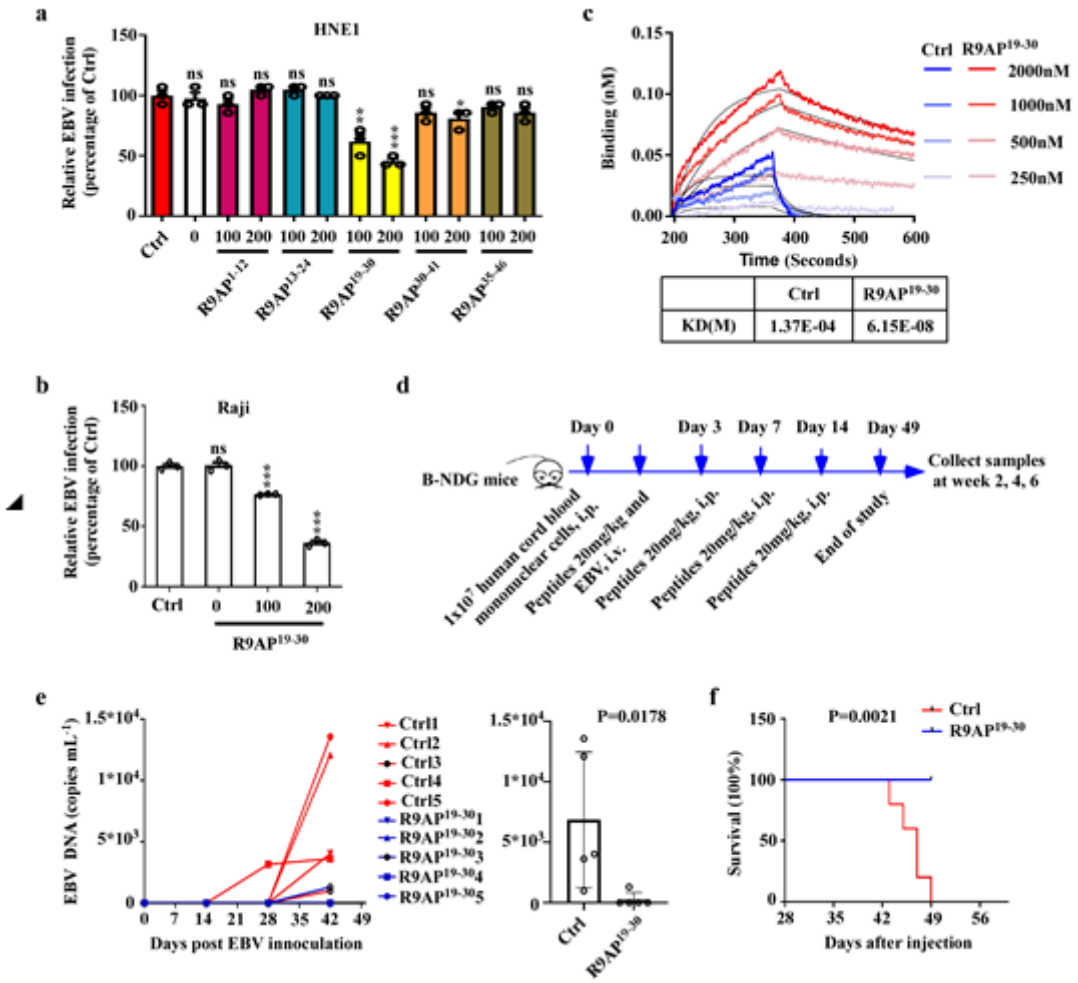

Figure 5

R9AP peptide inhibits EBV infection in vitro and in vivo. a, EBV was pretreated with indicated amount of R9AP1-12, R9AP13-24, R9AP19-30, R9AP30-41, R9AP35-46 or control peptide (Ctrl) for 2 h at 4°C then added to 5×104 HNE1 cells in 24–well plates and co-incubated for 3h at 37°C. Then, virus was removed, and EBV infection efficiency was analyzed by flow cytometry after 24h. Bars represent percentage of infection, with Ctrl-treated EBV infection of indicated cells was normalized to 100%. Results are expressed as mean ± s.e.m. from three independent experiments, two-tailed unpaired Student's t-test (ns, not significant; *P < 0.05; **P < 0.01; ***P < 0.001). b, His-gH/gL proteins were captured onto Ni-NTA biosensors and assayed for binding to Ctrl or R9AP19-30 at the indicated concentrations. Kinetic values calculated from the fit model for binding curves were shown below the graph. c, R9AP19-30 or Ctrl pretreated EBV was added to 1×105 Raji cells, performed as in (a). Results are expressed as mean ± s.e.m. from three independent experiments, two-tailed unpaired Student's t-test (***P < 0.001). d,

Schematic representation of in vivo EBV infection using humanized B-NDG mice. B-NDG mice were injected intraperitoneally human cord blood mononuclear cells, each mouse was then treated with 30,000 infectious particles of EBV and indicated amounts of Ctrl or R9AP19-30 peptide. e, The copy number of EBV DNA in the blood of R9AP19-30 or control peptide-treated humanized B-NDG mice were determined by qPCR at indicated time points shown for each mouse (left) or for each treatment group of mice at 6th week (right). n=5 mice each group. P value calculated using unpaired two-tailed t-test. f, The survival of R9AP19-30 or control peptide-treated humanized B-NDG mice was recorded. P value was 0.0021, Log-Rank test.

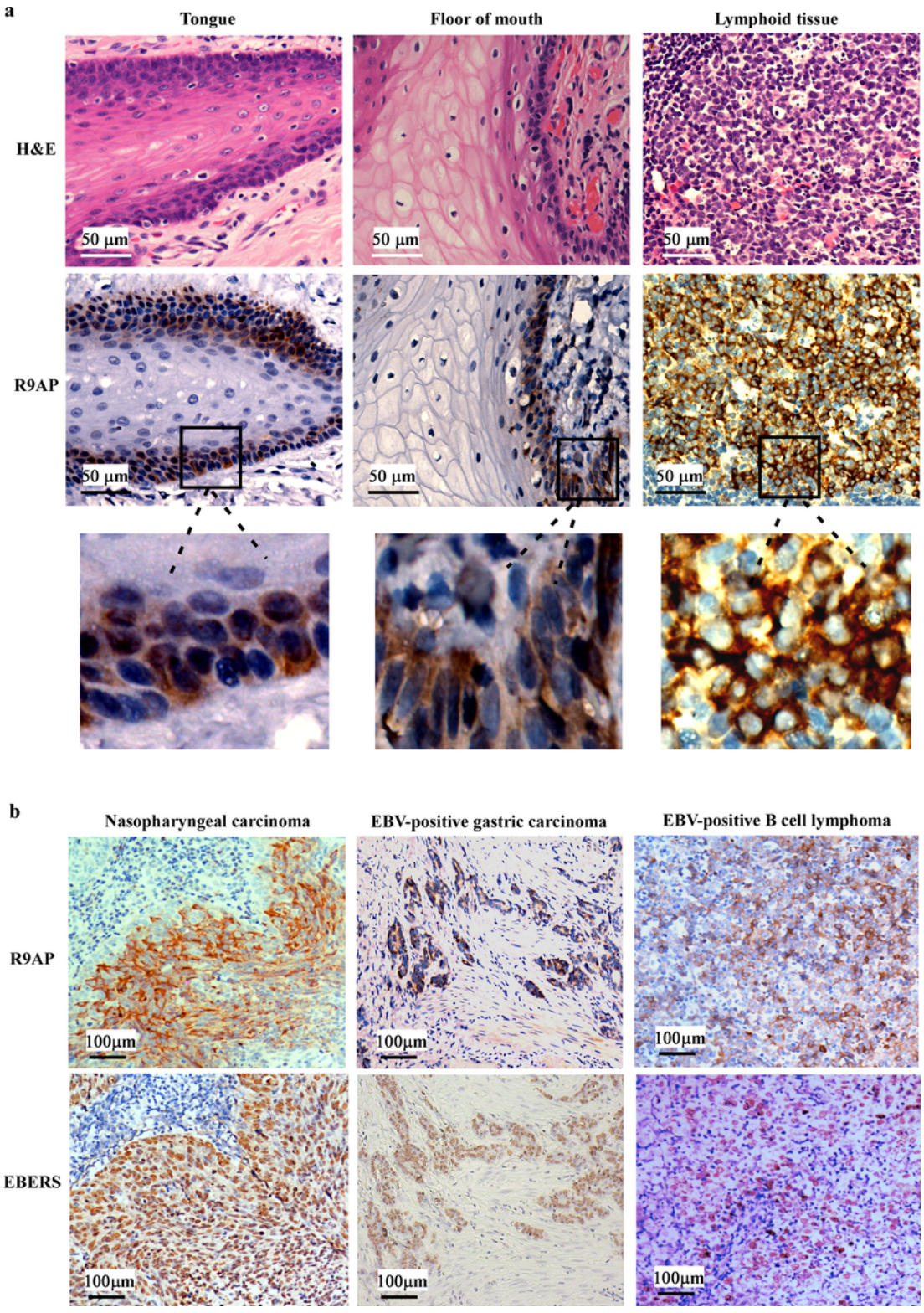

Figure 6

R9AP expression in human tissues susceptible to EBV infection. a, Human tongue, floor of mouth, and lymphoid tissues were stained with hematoxylin-eosin staining (H&E) (top row) and R9AP antibody (middle row). . Images of insets were magnified 4 times (bottom row). Scale bars: 50 □m. b, Nasopharyngeal carcinoma, gastric carcinoma and B cell lymphomas were stained with human R9AP antibody (top row) or with EBV EBERs probe (bottom row). Scale bars: 100 □m.

Supplementary Files

This is a list of supplementary files associated with this preprint. Click to download.

- SupplementaryTable1.xlsx
- SupplementaryFigures.docx